

## PROJECTION-BASED MODEL REDUCTION FOR FINITE ELEMENT APPROXIMATION OF SHALLOW WATER FLOWS

Matthew Farthing<sup>1</sup>, Alexander Lozovskiy<sup>2</sup>, and Chris Kees<sup>1</sup>

<sup>1</sup>Coastal and Hydraulics Laboratory, U.S. Army Engineer Research and Development Center,  
3909 Halls Ferry Road, Vicksburg, MS 39180, USA  
e-mail: matthew.w.farthing@usace.army.mil

<sup>2</sup>Institute of Scientific Computation, Texas A&M University,  
155 Ireland Street, College Station, TX 77840, USA  
e-mail: lozovskiy@math.tamu.edu

**Keywords:** Shallow Water equations, model reduction, POD, GNAT, global basis.

**Abstract.** *The shallow water equations (SWE) are used to model a wide range of environmental flows from dam breaks and riverine hydrodynamics to hurricane storm surge and atmospheric processes. Despite significant gains in numerical model efficiency stemming from algorithmic and hardware improvements, accurate shallow water modeling can still be very computationally intensive. The resulting computational expense remains as a barrier to the inclusion of fully resolved two-dimensional shallow water models in many applications, particularly when the analysis involves optimal design, parameter inversion, risk assessment, and/or uncertainty quantification.*

*Here, we consider projection-based model reduction as a way to alleviate the computational burden associated with high-fidelity shallow-water approximations in ensemble forecast and sampling methodologies. In order to develop a robust approach that can resolve advection-dominated problems with shocks as well as more smoothly varying riverine and estuarine flows, we consider techniques using both Galerkin and Petrov-Galerkin projection on global bases provided by Proper Orthogonal Decomposition (POD). To achieve realistic speedup, we consider alternative methods for the reduction of the non-polynomial nonlinearities that arise in typical finite element formulations. We evaluate the schemes' performance by considering their accuracy and robustness for test problems in one and two space dimensions.*

## 1 INTRODUCTION

The two-dimensional, depth-averaged shallow water equations (SWE) are used throughout science and engineering to model free-surface flows in systems where vertical scales are small with respect to horizontal length scales [22]. Their widespread utility has led to the development of a host of numerical methods and solution techniques for the SWE. A non-exhaustive list includes high-resolution finite volume [18] and discontinuous Galerkin methods [1] as well as characteristic-based [21] and stabilized finite element methods (FEMs) [7].

While ongoing work continues to improve the performance of core numerical methods for the SWE, it is clear that alternative approaches are needed to achieve the speedups necessary to make use of the SWE common in real-time simulation or sampling-intensive methods for risk assessment or uncertainty quantification [9]. Here, we consider global model reduction for the SWE via projection. Specifically, we consider Galerkin-based projection via Proper Orthogonal Decomposition (POD) [3] as well as Petrov-Galerkin approximations based on the Gauss-Newton with Approximate Tensors (GNAT) technique introduced by [11, 12]. In both cases, we use a series of high-fidelity training simulations (or snapshots) in an offline stage to build a basis of empirical modes using a Singular Value Decomposition (SVD) for the solution in order to capture flow dynamics using (hopefully) many fewer degrees of freedom than the original, high-fidelity simulation. Calculations using this low-dimensional or reduced basis can then, in principle, be performed much faster during a time or resource sensitive online stage [3].

Due to the non-polynomial nonlinearities that arise in standard roughness parameterizations and stabilized FEM approximations, further reduction of the nonlinearities in the SWE are required to break dependence on the fine-scale dimension [2]. We evaluate two types of so-called hyper-reduction for our reduced models: Discrete Empirical Interpolation (DEIM) [5, 13] and gappy POD [14, 23].

In the following, we lay out these reduction techniques for a semi-implicit, stabilized FEM approximation of the SWE. We pay particular attention to conditions when the schemes are *consistent*. That is, we consider conditions under which the models will restore the original fine-scale solution if the entire empirical basis obtained from the snapshot collection is used [11]. We end with numerical experiments comparing performance of the various methods for a one-dimensional Burgers equation problem as well as a two-dimensional dam-break.

## 2 HIGH-FIDELITY FORMULATION FOR THE SHALLOW WATER EQUATIONS

### 2.1 Continuous formulation

We begin with the fine scale formulation. The standard two-dimensional shallow water equations consist of a mass conservation equation and two scalar momentum conservation equations that can be written in conservative form as

$$\frac{\partial \mathbf{u}}{\partial t} + \nabla \cdot (\mathbf{F} - \mathbf{D} \nabla \mathbf{u}) + \mathbf{r} = 0, \quad (1)$$

where

$$\mathbf{u} \equiv \begin{pmatrix} u_1 \\ u_2 \\ u_3 \end{pmatrix} = \begin{pmatrix} h \\ hu \\ hv \end{pmatrix}$$

Here,  $h \geq 0$  is the total depth of the water column and the velocity components in the  $x$  and  $y$  directions are  $u$  and  $v$ , respectively. We assume (1) holds over a domain  $\Omega \subset \mathbb{R}^2$  with outward

normal  $\mathbf{n}$  and spatially varying bathymetry represented by a function  $b(x, y)$  that is strictly negative.

The flux matrix  $\mathbf{F}(\mathbf{u})$  and diffusion tensor in (1) have the form

$$\mathbf{F} = \begin{pmatrix} u_2 & u_3 \\ \frac{u_2^2}{u_1} + \frac{gu_1^2}{2} & \frac{u_2u_3}{u_1} \\ \frac{u_2u_3}{u_1} & \frac{u_3^2}{u_1} + \frac{gu_1^2}{2} \end{pmatrix}, \quad \mathbf{D} = \begin{pmatrix} 0 & 0 & 0 \\ 0 & \nu & 0 \\ 0 & 0 & \nu \end{pmatrix}$$

with turbulent viscosity  $\nu$ , and gravitational acceleration  $g$ . The source term  $\mathbf{r}(\mathbf{u})$  contains the topography gradient and the Manning's bed friction term with coefficient  $n_{mn}$

$$\mathbf{r} = gh \begin{pmatrix} 0 \\ \frac{\partial b}{\partial x} \\ \frac{\partial b}{\partial y} \end{pmatrix} + gn_{mn}^2 \frac{\sqrt{u_2^2 + u_3^2}}{u_1^{\frac{7}{3}}} \begin{pmatrix} 0 \\ u_2 \\ u_3 \end{pmatrix}.$$

Note that the fluid surface elevation is defined as  $\eta = u_1 + b$ , and the discharge is  $(hu, hv)^T$ . Everywhere below, we assume that  $b$  has as much continuity as required.

We assume that initial conditions  $h^0(x, y)$ ,  $u^0(x, y)$  and  $v^0(x, y)$  are specified for  $h, u$ , and  $v$ , respectively. For simplicity, we do not assume any Dirichlet boundary conditions for (1). Instead, we impose that  $\mathbf{D}\nabla\mathbf{u} \cdot \mathbf{n} = 0$  on  $\partial\Omega$  and, possibly, that  $u_2n_x + u_3n_y = 0$  on portions of  $\partial\Omega$  where no discharge is expected.

## 2.2 Stabilized Finite Element scheme

The classical finite element scheme for equation (1) with the considered boundary conditions relies on the following exact weak formulation. If  $\mathbf{w}$  denotes an arbitrary test function from a reasonable test space, then

$$\int_{\Omega} \frac{\partial \mathbf{u}}{\partial t} \cdot \mathbf{w} - \int_{\Omega} \mathbf{F} \cdot \nabla \mathbf{w} + \int_{\Omega} \mathbf{D} \nabla \mathbf{u} \cdot \nabla \mathbf{w} + \int_{\Omega} \mathbf{r} \cdot \mathbf{w} + \int_{\partial\Omega} (\mathbf{F} \cdot \mathbf{n}) \cdot \mathbf{w} = 0 \quad (2)$$

In the above, the first component of  $\mathbf{F} \cdot \mathbf{n}$  in the boundary integral term is zero whenever the boundary condition  $u_2n_x + u_3n_y = 0$  is imposed.

Let  $\phi_j$  denote the  $j$ -th scalar shape function from a standard space of piecewise linear functions on a conformal mesh of  $\Omega$  with  $N_n$  nodes. We can then approximate the components  $u_i$  of our solution in (2) via

$$u_i \approx u_i^h = \sum_{j=1}^{N_n} \phi_j v_i^j, \quad (3)$$

where  $1 \leq i \leq 3$  refers to the unknown of (1) and  $1 \leq j \leq N_n$ . We label the trial space for the full unknown  $\mathbf{u}^h$  as  $\mathbf{V}_h$ . Setting  $\mathbf{w}^h$  to all of the available basis functions  $\mathbf{w}_j^h$  from  $\mathbf{W}_h = \mathbf{V}_h$  in (2), together with (3), yields a time-dependent nonlinear system of  $N = 3N_n$  ordinary differential equations (semi-discrete scheme):

$$\begin{aligned} & \int_{\Omega} \frac{\partial \mathbf{u}^h}{\partial t} \cdot \mathbf{w}_j^h - \int_{\Omega} \mathbf{F}(\mathbf{u}^h) \cdot \nabla \mathbf{w}_j^h + \int_{\Omega} \mathbf{D} \nabla \mathbf{u}^h \cdot \nabla \mathbf{w}_j^h + \\ & \int_{\Omega} \mathbf{r}(\mathbf{u}^h) \cdot \mathbf{w}_j^h + \int_{\partial\Omega} (\mathbf{F}(\mathbf{u}^h) \cdot \mathbf{n}) \cdot \mathbf{w}_j^h = 0, \quad j = 1, \dots, 3N_n \end{aligned} \quad (4)$$

Regardless of the time discretization employed for (4), the system in general suffers from convection- and shock-type instabilities, especially for small viscosity  $\nu$  or insufficient mesh resolution [15, 16], and calls for additional stabilization terms. Letting  $a(\cdot, \cdot)$  denote the standard Galerkin approximation for the stationary part of (4), a generalization of classical SUPG stabilization via Hughes variational multiscale paradigm [16] can be written as

$$\int_{\Omega} \frac{\partial \mathbf{u}^h}{\partial t} \cdot \mathbf{w}^h + a(\mathbf{u}^h, \mathbf{w}^h) + \sum_e \int_{\Omega_e} \mathcal{M}_{\mathbf{u}^h} \mathbf{w}^h \cdot \boldsymbol{\tau} \mathbf{R}_h(\mathbf{u}^h) = 0, \quad (5)$$

where the vector operator  $\mathcal{M}_{\mathbf{u}^h}$  is

$$\mathcal{M}_{\mathbf{u}^h} \mathbf{w}^h = - \sum_i \left( \mathbf{A}_{h,i}(\mathbf{u}^h)^T \frac{\partial \mathbf{w}^h}{\partial x_i} \right) + \frac{\partial \mathbf{r}^T}{\partial \mathbf{u}}(\mathbf{u}^h) \mathbf{w}^h \quad (6)$$

and  $\mathbf{A}_{h,i}(\mathbf{u}^h)$  for  $i = 1, 2$  are advection matrices

$$\mathbf{A}_{h,i}(\mathbf{u}^h) = \frac{\partial \mathbf{F}_i}{\partial \mathbf{u}}(\mathbf{u}^h) \quad (7)$$

and  $\mathbf{F}_i$  denotes the  $i$ -th column of the matrix  $\mathbf{F}$ . Here  $\boldsymbol{\tau}$  is a matrix of intrinsic time scales that can be specified using an algebraic subgrid scale (ASGS) approach [20].  $\mathbf{R}_h(\mathbf{u}^h)$  denotes the residual of the continuous formulation (1) (so-called strong residual),  $x_1 = x$ ,  $x_2 = y$ , and  $\mathbf{w}^h$  represents a discrete test function taken from  $\mathbf{W}_h$ .

For problems with strong nonlinearities and sharp fronts, we resort to adding a shock-capturing term having a form of an artificial viscosity [8]:

$$\sum_e \int_{\Omega_e} c_{sh} \frac{h_e}{2} \frac{\|\mathbf{R}_h(\mathbf{u}^h)\|}{\|\nabla \mathbf{u}^h\| + \delta} \nabla \mathbf{u}^h \cdot \nabla \mathbf{w}^h \quad (8)$$

where  $h_e$  denotes the characteristic width of an element  $\Omega_e$  and  $c_{sh}$  is a positive scaling constant usually taken to be less than 1 and all the norms are standard 2-norms. Note that  $\mathbf{R}_h$  does not contain diffusive terms since we are using piecewise linear shape functions, and small term  $\delta$  is added to separate the denominator from zero.

**Remark 1.** *In the following, we consider stabilization only through the nonlinear shock-capturing term (8), which in our experience is the dominant term for controlling instabilities due to sharp fronts and shocks. While simplifying the implementation, the reduction schemes presented here apply to the fine-scale scheme from [20] with only minor differences.*

The final form of our finite element scheme for the high-fidelity simulations is

$$\begin{aligned} & \int_{\Omega} \frac{\partial \mathbf{u}^h}{\partial t} \cdot \mathbf{w}^h - \int_{\Omega} \mathbf{F}(\mathbf{u}^h) \cdot \nabla \mathbf{w}^h + \int_{\Omega} \mathbf{D} \nabla \mathbf{u}^h \cdot \nabla \mathbf{w}^h + \int_{\Omega} \mathbf{r}(\mathbf{u}^h) \cdot \mathbf{w}^h + \\ & \int_{\partial \Omega} (\mathbf{F}(\mathbf{u}^h) \cdot \mathbf{n}) \cdot \mathbf{w}^h + \sum_e \int_{\Omega_e} c_{sh} \frac{h_e}{2} \frac{\|\mathbf{R}_h(\mathbf{u}^h)\|}{\|\nabla \mathbf{u}^h\| + \delta} \nabla \mathbf{u}^h \cdot \nabla \mathbf{w}^h = 0. \end{aligned} \quad (9)$$

The semi-discrete approximation in equation (9), expressed as a system of ordinary differential equations, can be viewed as

$$\mathbf{M} \dot{\mathbf{v}} + \mathbf{L} \mathbf{v} + \mathbf{f}(\mathbf{v}) = 0 \quad (10)$$

with solution  $\mathbf{v} = (\mathbf{v}_1^T, \mathbf{v}_2^T, \mathbf{v}_3^T)^T$  consisting of the degrees of freedom for the approximate solution  $\mathbf{u}^h$  and  $\mathbf{f} = (\mathbf{f}_1^T, \mathbf{f}_2^T, \mathbf{f}_3^T)^T$ . The term  $\mathbf{f}$  comprises all the nonlinear terms of equation (9), including those with nonlinear stabilization. The vector components  $\mathbf{f}_2$  and  $\mathbf{f}_3$  also involve boundary integrals. Matrix  $\mathbf{L}$  of the linear term is based on the diffusion and topography terms, and in the case of outflow boundaries may also contain the first component of  $\int_{\Omega} (\mathbf{F} \cdot \mathbf{n}) \cdot \mathbf{w}$ .  $\mathbf{M}$  is a standard mass matrix.

### 2.3 Time discretization

For marching in time from  $t_0 = 0$  with a variable time step,  $\Delta t_k$ , we construct the fully discrete scheme using the first-order Euler approximation (higher order backward difference schemes can be used to increase accuracy in time). In order to avoid solving a large nonlinear algebraic system at each time step, a semi-implicit variant of the fully implicit scheme is proposed in such a way that extrapolation is introduced inside all nonlinear terms in (9). This lagging does not influence the accuracy of the scheme, but makes it only conditionally stable [17]. Everywhere below, any discrete in time function  $\mathbf{f}$  at time level  $k$  is denoted as  $\mathbf{f}^k$ .

The resulting fine-scale linear system to be solved has the schematic form

$$\left( \underbrace{\frac{1}{\Delta t_k} \mathbf{M} + \mathbf{L}}_{\mathbf{A}} + \underbrace{\begin{pmatrix} \mathbf{N}_{11} & \mathbf{0} & \mathbf{0} \\ \mathbf{N}_{21} & \mathbf{N}_{22} & \mathbf{N}_{23} \\ \mathbf{N}_{31} & \mathbf{N}_{32} & \mathbf{N}_{33} \end{pmatrix}}_{\mathbf{N}} \right)^{k-1, k-2} \begin{pmatrix} \mathbf{v}_1 \\ \mathbf{v}_2 \\ \mathbf{v}_3 \end{pmatrix}^k = \frac{1}{\Delta t_k} \mathbf{M} \begin{pmatrix} \mathbf{v}_1 \\ \mathbf{v}_2 \\ \mathbf{v}_3 \end{pmatrix}^{k-1}. \quad (11)$$

Block  $\mathbf{N}_{ij}$  corresponds to test function component  $w_i$  and solution component  $u_j$ . Note that the shock-capturing and the Manning friction terms only contribute to the diagonal terms of  $\mathbf{N}$ . Every block  $\mathbf{N}_{ij}$  depends on the solution and has to be reassembled after every time step. Just for the first time step, we set  $c_{sh} = 0$ , as no information is given regarding  $\mathbf{u}^{-1}$  in the mass part of the shock-capturing term, and so  $\mathbf{N}$  depends on  $\mathbf{v}^0$  only. In the case of strong Dirichlet boundary conditions, we include an additional vector  $\mathbf{v}_d$  containing the boundary values to the right hand side and modify  $\mathbf{A}$  and  $\mathbf{N}_{ij}$ ,  $i, j = 1, 2, 3$  accordingly.

## 3 GLOBAL BASIS REDUCED ORDER MODEL FRAMEWORK

The fine-scale approximation above allows calculation of a numerical solution that improves with mesh refinement. We assume that computational resources in the offline stage are sufficient to allow the temporal and spatial resolution necessary to resolve all relevant solution features. We then focus on the online stage where computational resources and/or time-constraints dictate that a much faster (i.e., reduced) model with possibly relaxed accuracy is needed. We first present the basic methodology for the reduction relying on a global empirical basis representing the coherent structures of the fine-scale processes. We use a generic algebraic formulation typical of semi-implicit temporal approximations without making specific reference to the SWE.

### 3.1 Proper Orthogonal Decomposition of the state variable for semi-implicit schemes

POD is probably the best-known projection-based model reduction scheme. It has been applied to a host of general, large-scale parameterized dynamical systems. Fundamentally, it is based on approximating the high-dimensional solution to the dynamical system in a low-dimensional subspace that is chosen by considering modes that capture a targeted portion of the system's energy [4, 10]. To obtain a dynamical system of low dimension, POD proceeds by

projecting the original high-dimensional equations on the solution subspace. Since it uses the same subspace for both the solution and projection steps, POD can be considered as a (Bubnov) Galerkin method [12].

Consider the following semi-implicit Euler discretization with variable time step  $\Delta t_i$  aimed at connecting the state variable at time level  $i$  with time levels  $i-1$ ,  $i-2$  that represents (among others) our current SWE scheme:

$$\mathbf{R}^i \equiv (\mathbf{A}^i + \mathbf{N}(\mathbf{v}^{i-2}, \mathbf{v}^{i-1}))\mathbf{v}^i - \Delta t_i^{-1} \mathbf{M} \mathbf{v}^{i-1} - \mathbf{d}^i = 0,$$

Here  $\mathbf{R}$  denotes the residual of the fully discrete approximation. Matrix  $\mathbf{A}^i$  comprises matrices from all the linear terms containing the solution at time level  $i$  and depends only  $\Delta t^i$ , while  $\mathbf{N}$  consists of the matrices constructed through extrapolating the solution at previous time levels  $i-2, i-1$  to the time level  $i$  in the nonlinear terms. Term  $\mathbf{d}^i$  accounts for the external source and the boundary conditions data at level  $i$  and is state-independent. Again, such extrapolation is a common technique behind semi-implicit schemes that retains (theoretically) the same order of accuracy as for the fully implicit approximation, though in general it is not unconditionally stable.

To initiate the time integration, we assume that  $\mathbf{v}^0$  is given at time level 0 via projection of the initial condition and that  $\mathbf{N}(\mathbf{v}^{-1}, \mathbf{v}^0)$  is replaced with  $\mathbf{N}_0(\mathbf{v}^0)$  for the first time step only. Therefore, we have the following fine-scale, fully discrete problem statement within the semi-implicit paradigm:

$$\begin{cases} \text{initial data } \mathbf{v}^0 \text{ given,} \\ (\mathbf{A}^0 + \mathbf{N}_0(\mathbf{v}^0))\mathbf{v}^1 - \Delta t_1^{-1} \mathbf{M} \mathbf{v}^0 - \mathbf{d}^1 = 0, \\ (\mathbf{A}^i + \mathbf{N}(\mathbf{v}^{i-2}, \mathbf{v}^{i-1}))\mathbf{v}^i - \Delta t_i^{-1} \mathbf{M} \mathbf{v}^{i-1} - \mathbf{d}^i = 0, \quad i \geq 2 \end{cases} \quad (12)$$

We define  $\mathbf{S} = (\mathbf{v}^1, \mathbf{v}^2, \dots, \mathbf{v}^M)$  to be an  $N \times M$  matrix of solution snapshots,  $M \leq N$ , obtained from the high precision offline runs from  $t = 0$  to  $t = T$  for the state variable  $\mathbf{v}$ . Note, that we do not include the initial data into the snapshot set. In practice, the set  $\mathbf{S}$  may consist of snapshots at intermediate values of  $t$  from  $[0, T]$ , for each corresponding input parameter or forcing function. Also, unlike [12], we store solution values rather than increments, which will be shown to be adequate for the semi-implicit scheme above.

A thin SVD is used for the matrix of snapshots to achieve the sought basis:

$$\mathbf{S} = \mathbf{U} \text{diag}(\sigma_1, \dots, \sigma_M) \mathbf{Q}^T, \quad (13)$$

with  $\sigma_i$  denoting the singular values in decreasing order,  $\sigma_1 \geq \sigma_2 \geq \dots \geq \sigma_M \geq 0$ . Both  $\mathbf{U}$  and  $\mathbf{Q}$  consist of orthonormal vectors that satisfy

$$\mathbf{S}^T \mathbf{S} \mathbf{q}^j = (\sigma_j)^2 \mathbf{q}^j, \quad \mathbf{S} \mathbf{S}^T \mathbf{u}_j = (\sigma_j)^2 \mathbf{u}_j.$$

The columns  $\mathbf{u}_j$  of the matrix  $\mathbf{U} \in \mathbb{R}^{N \times M}$  provide the desired basis vectors, also called the *empirical modes* for the solution  $\mathbf{v}$ . They are ordered correspondingly with  $\sigma_j$ .

The use of the reduced-order approach is justified when we connect the reduced-order discrete solution  $\mathbf{z}$  of size  $m \leq M$  to the high-fidelity discrete solution via the approximation

$$\mathbf{v} \approx \mathbf{U}_r \mathbf{z}, \quad (14)$$

where  $\mathbf{U}_r$  denotes the submatrix of  $\mathbf{U}$  consisting only of the first  $m$  columns of  $\mathbf{U}$  and  $m \ll N$ . Plugging this approximation into the original semi-discrete system makes it over-determined in general. Indeed, denote the approximate residual at time level  $i$  as

$$\mathbf{R}_r(\mathbf{z}^i) \equiv (\mathbf{A}^i + \mathbf{N}(\mathbf{U}_r \mathbf{z}^{i-2}, \mathbf{U}_r \mathbf{z}^{i-1})) \mathbf{U}_r \mathbf{z}^i - \Delta t_i^{-1} \mathbf{M} \mathbf{U}_r \mathbf{z}^{i-1} - \mathbf{d}^i. \quad (15)$$

Unlike the original high-dimensional model, this residual is not necessarily zero, due to non-exactness of (14). Thus some form of projection is required to reduce the number of the resulting equations, i.e., multiplication from the left by a full rank matrix of size  $m \times N$ . We consider two alternative approaches, namely a standard Galerkin (POD) projection as well as a Petrov-Galerkin projection [6, 12].

### 3.1.1 Galerkin projection

Standard Galerkin projection uses left multiplication by some constant (time and state-independent) matrix  $\mathbf{V}^T$ . The benefits of this approach stem directly from the fact that  $\mathbf{V}^T$  is constant and allows for pre-assembly of various components of the reduced-order model that do not require update at every time step. The drawback is in that such projection is not based on an optimality criterion. Usually, a Bubnov-Galerkin approach is used in which  $\mathbf{V} = \mathbf{U}_r$ , but we consider arbitrary full-rank  $\mathbf{V}$  to allow some flexibility. The reduced-order model relying on the Galerkin projection then takes the form

$$\mathbf{V}^T (\mathbf{A}^i + \mathbf{N}(\mathbf{U}_r \mathbf{z}^{i-2}, \mathbf{U}_r \mathbf{z}^{i-1})) \mathbf{U}_r \mathbf{z}^i - \Delta t_i^{-1} \mathbf{V}^T \mathbf{M} \mathbf{U}_r \mathbf{z}^{i-1} - \mathbf{V}^T \mathbf{d}^i = 0, \quad (16)$$

The above system will have a unique solution  $\mathbf{z}^i$  at every time step  $i$ , provided the matrix  $\mathbf{V}^T (\mathbf{A}^i + \mathbf{N}(\mathbf{U}_r \mathbf{z}^{i-2}, \mathbf{U}_r \mathbf{z}^{i-1})) \mathbf{U}_r^T$  always remains non-singular. When  $\mathbf{V} = \mathbf{U}_r$ , this is equivalent to  $\mathbf{A}^i + \mathbf{N}(\mathbf{U}_r \mathbf{z}^{i-2}, \mathbf{U}_r \mathbf{z}^{i-1})$  being non-singular. With initial conditions taken into account, we obtain

$$\begin{cases} \text{initial data } \mathbf{v}^0 \text{ given,} \\ \mathbf{V}^T (\mathbf{A}^i + \mathbf{N}_0(\mathbf{v}^0)) \mathbf{U}_r \mathbf{z}^1 - \Delta t_1^{-1} \mathbf{V}^T \mathbf{M} \mathbf{v}^0 - \mathbf{V}^T \mathbf{d}^1 = 0, \\ \mathbf{V}^T (\mathbf{A}^i + \mathbf{N}(\mathbf{U}_r \mathbf{z}^{i-2}, \mathbf{U}_r \mathbf{z}^{i-1})) \mathbf{U}_r \mathbf{z}^i - \Delta t_i^{-1} \mathbf{V}^T \mathbf{M} \mathbf{U}_r \mathbf{z}^{i-1} - \mathbf{V}^T \mathbf{d}^i = 0, \quad i \geq 2 \end{cases} \quad (17)$$

In the last equation above, the notation  $\mathbf{U}_r \mathbf{z}^0$  is simply used for the initial data  $\mathbf{v}^0$  when  $i = 2$ . In the numerical experiments below, we will refer to (17) as the nonlinear POD (NPOD) approximation.

### 3.1.2 Petrov-Galerkin projection

We next consider a Petrov-Galerkin projection following the GNAT approach from [12]. Unlike the Galerkin (NPOD) approach above, it is constructed directly from the minimization considerations for the approximate residual at every time step. Considering (15), we pose the following problem at step  $i$ :

$$\mathbf{z}^i = \underset{\mathbf{z} \in \mathbb{R}^m}{\operatorname{argmin}} \|\mathbf{R}_r(\mathbf{z})\|$$

This problem is equivalent to a standard least-squares problem obtained through the left multiplication of equation (15) by the transpose of  $(\mathbf{A} + \mathbf{N})\mathbf{U}$  and setting the result to zero:

$$\begin{aligned} \mathbf{U}_r^T (\mathbf{A}^{i,T} + \mathbf{N}^T(\mathbf{U}_r \mathbf{z}^{i-2}, \mathbf{U}_r \mathbf{z}^{i-1})) (\mathbf{A}^i + \mathbf{N}(\mathbf{U}_r \mathbf{z}^{i-2}, \mathbf{U}_r \mathbf{z}^{i-1})) \mathbf{U}_r \mathbf{z}^i = \\ \mathbf{U}_r^T (\mathbf{A}^{i,T} + \mathbf{N}^T(\mathbf{U}_r \mathbf{z}^{i-2}, \mathbf{U}_r \mathbf{z}^{i-1})) (\Delta t^{-1} \mathbf{M} \mathbf{U}_r \mathbf{z}^{i-1} + \mathbf{d}^i) \end{aligned}$$

The above linear system for  $\mathbf{z}^i$  is typically solved through a Moore-Penrose pseudoinverse of the rectangular matrix  $(\mathbf{A} + \mathbf{N})\mathbf{U}_r$ .

Analogous to the Galerkin reduced-order model, we construct the following reduced-order initial value problem:

$$\begin{cases} \text{initial data } \mathbf{v}^0 \text{ given,} \\ \mathbf{z}^1 = \underset{\mathbf{z} \in \mathbb{R}^m}{\operatorname{argmin}} \|(\mathbf{A}^1 + \mathbf{N}_0(\mathbf{v}^0))\mathbf{U}_r\mathbf{z} - \Delta t_1^{-1}\mathbf{M}\mathbf{v}^0 - \mathbf{d}^1\|, \\ \mathbf{z}^i = \underset{\mathbf{z} \in \mathbb{R}^m}{\operatorname{argmin}} \|(\mathbf{A}^i + \mathbf{N}(\mathbf{U}_r\mathbf{z}^{i-2}, \mathbf{U}_r\mathbf{z}^{i-1}))\mathbf{U}_r\mathbf{z} - \Delta t_i^{-1}\mathbf{M}\mathbf{U}_r\mathbf{z}^{i-1} - \mathbf{d}^i\|, \quad i \geq 2 \end{cases} \quad (18)$$

We will refer to (18) as the nonlinear Petrov-Galerkin (PG-NPOD) approximation below.

### 3.1.3 Consistency

As mentioned above, consistency is a desirable property for projection-based reduced-order models, since a consistent reduced order model will restore the fine-scale solution precisely when the entire empirical basis is used (that is, there is no truncation, meaning  $\mathbf{U}_r = \mathbf{U}$ ). It can be shown that both the Galerkin (17) and Petrov-Galerkin (18) models are consistent under suitable assumptions on the time step selection and invertibility of the iteration matrices.

### 3.1.4 Multiple variables

For systems of PDEs, involving more than one variable (such as, for example, the shallow water system), it is a common strategy to collect separate snapshots sets for each of the solution components, to have more control over reduction errors corresponding to certain variables. For situations involving  $n$  variables, we construct  $n$  snapshot matrices  $\mathbf{S}_j$ ,  $1 \leq j \leq n$ , corresponding to the same time instances, and apply the SVD procedure to each of them separately. The calculated bases  $\mathbf{U}_j$  are then grouped block-wise along the diagonal for the global basis  $\mathbf{U}$ :

$$\mathbf{U} = \begin{pmatrix} \mathbf{U}_1 & 0 & \cdots & 0 \\ 0 & \mathbf{U}_2 & \cdots & 0 \\ \vdots & \vdots & \ddots & \vdots \\ 0 & 0 & \cdots & \mathbf{U}_n \end{pmatrix} \quad (19)$$

The truncation can then be done for each variable independently. In this case, when the whole bases  $\mathbf{U}_j$  are used for all of the variables in the reduced-order models a consistency result can be shown for Galerkin projection via a constant, full-rank (not necessarily block-diagonal) matrix  $\mathbf{V}^T$  and Petrov-Galerkin projection. This is due to the fact that every snapshot for the  $i$ -th variable belongs to  $\operatorname{range}(\mathbf{U}_i)$  for all  $M$  time levels.

## 3.2 Hyper-reduction for Galerkin projection

For reduced models based on Galerkin projection, precomputation of the constant matrix factor  $\mathbf{V}^T\mathbf{M}\mathbf{U}_r$  can be done only once before marching in time and therein be used for cheap multiplication by  $\mathbf{z}^{i-1}$  in equation (17) at every time step. Precomputation (with scalar multiplication) can also be done for the term  $\mathbf{V}^T\mathbf{A}^i\mathbf{U}_r$ . Unfortunately, the nonlinear piece  $\mathbf{V}^T\mathbf{N}(\mathbf{U}_r\mathbf{z}^{i-2}, \mathbf{U}_r\mathbf{z}^{i-1})\mathbf{U}_r$  requires recomputation in the original high-dimensional space and subsequent projection back to the reduced space at every time step. Such computational burden, involving operations with



complexity that scales linearly with the order  $N$  of the high-dimensional space, diminishes the execution speedup achieved by state reduction. To overcome this performance issue, further complexity reduction — this time applied to the terms calling for update at every step — is required.

To achieve this, we will consider hyper-reduction [2, 6]. The hyper-reduction approaches we consider rely on the same paradigm of expansion through a basis as we use for the solution state itself. We begin by constructing an additional snapshot matrix  $\mathbf{T}$  for the nonlinear portion of the discrete residual during the offline stage. In the semi-implicit scheme (17), this corresponds to the action of the nonlinear part of the left-hand-side (LHS) matrix on the state vector  $\mathbf{N}\mathbf{U}_r\mathbf{z}^i$ . The aim of collecting these snapshots is to capture the range of the entire nonlinear portion with a corresponding global, empirical (SVD) basis denoted as  $\mathbf{W}$ . To be specific, during the run of the state-reduced model with fixed basis  $\mathbf{U}_r$ , the following snapshot set is accumulated during  $M$  time steps:

$$\mathbf{T}^G = (\mathbf{N}_0(\mathbf{v}^0)\mathbf{U}_r\mathbf{z}^1, \mathbf{N}(\mathbf{v}^0, \mathbf{U}_r\mathbf{z}^1)\mathbf{U}_r\mathbf{z}^2, \dots, \mathbf{N}(\mathbf{U}_r\mathbf{z}^{M-2}, \mathbf{U}_r\mathbf{z}^{M-1})\mathbf{U}_r\mathbf{z}^M) \quad (20)$$

The empirical basis  $\mathbf{W}$  is then found via SVD as  $\mathbf{T}^G = \mathbf{W}\text{diag}(\bar{\sigma}_1, \bar{\sigma}_2, \dots, \bar{\sigma}_M)\bar{\mathbf{Q}}^T$ . With this basis, we then attempt to approximate  $\mathbf{N}\mathbf{U}_r\mathbf{z}^i$  as

$$\mathbf{N}(\mathbf{U}_r\mathbf{z}^{i-2}, \mathbf{U}_r\mathbf{z}^{i-1})\mathbf{U}_r\mathbf{z}^i \approx \mathbf{W}_r\mathbf{c}^i$$

via a time-dependent coefficient vector  $\mathbf{c}^i$ , where  $\mathbf{W}_r$  is a column-reduced submatrix from  $\mathbf{W}$ . The best possible approximation of such type in the standard 2-norm is a projection  $\mathbf{c}^i = \mathbf{W}_r^T \mathbf{N}(\mathbf{U}_r\mathbf{z}^{i-2}, \mathbf{U}_r\mathbf{z}^{i-1})\mathbf{U}_r\mathbf{z}^i$ . This procedure, however, has no computational benefit, since it employs the computation of the entire  $N$ -dimensional vector. Two ways to avoid this pitfall are presented below.

As mentioned above, the two methods we consider for choosing  $\mathbf{c}^i$  are DEIM [13] and gappy POD [14, 23]. Both rely on approximating nonlinearities at a collection of  $l_w$  indices. DEIM takes a collocation approach and uses the approximation

$$\mathbf{N}(\mathbf{U}_r\mathbf{z}^{i-2}, \mathbf{U}_r\mathbf{z}^{i-1})\mathbf{U}_r\mathbf{z}^i \approx \mathbf{W}_r(\mathbf{P}^T\mathbf{W}_r)^{-1} \underbrace{\mathbf{P}^T\mathbf{N}(\mathbf{U}_r\mathbf{z}^{i-2}, \mathbf{U}_r\mathbf{z}^{i-1})\mathbf{U}_r\mathbf{z}^i}_{\text{cheap evaluation}}$$

where  $\mathbf{P}$  is a sampling (or permutation) matrix. Gappy POD instead uses a least squares reconstruction to approximate the nonlinear term as

$$\mathbf{N}(\mathbf{U}_r\mathbf{z}^{i-2}, \mathbf{U}_r\mathbf{z}^{i-1})\mathbf{U}_r\mathbf{z}^i \approx \mathbf{W}_r(\mathbf{P}^T\mathbf{W}_r)^+ \underbrace{\mathbf{P}^T\mathbf{N}(\mathbf{U}_r\mathbf{z}^{i-2}, \mathbf{U}_r\mathbf{z}^{i-1})\mathbf{U}_r\mathbf{z}^i}_{\text{cheap evaluation}}$$

Here  $(\mathbf{P}^T\mathbf{W}_r)^+$  is the Moore-Penrose pseudoinverse. DEIM requires that the number of sampling indices  $l_w = n_w$ , while gappy POD requires  $l_w \geq n_w$ . In the case of  $l_w = n_w$ , the approaches are identical assuming the same set of indices are used [20].

Defining the matrix  $\mathbf{G} = \mathbf{V}^T\mathbf{W}_r(\mathbf{P}^T\mathbf{W}_r)^{-1}$  or  $\mathbf{G} = \mathbf{V}^T\mathbf{W}_r(\mathbf{P}^T\mathbf{W}_r)^+$  in the case of DEIM and gappy POD, respectively, we can write the hyper-reduced Galerkin model as

$$\begin{cases} \text{initial data } \mathbf{v}^0 \text{ given,} \\ (\mathbf{V}^T\mathbf{A}^1\mathbf{U}_r + \mathbf{G}\mathbf{P}^T\mathbf{N}_0(\mathbf{v}^0)\mathbf{U}_r)\bar{\mathbf{z}}^1 - \Delta t_1^{-1}\mathbf{V}^T\mathbf{M}\mathbf{v}^0 - \mathbf{V}^T\mathbf{d}^1 = 0, \\ (\mathbf{V}^T\mathbf{A}^i\mathbf{U}_r + \mathbf{G}\mathbf{P}^T\mathbf{N}(\mathbf{U}_r\bar{\mathbf{z}}^{i-2}, \mathbf{U}_r\bar{\mathbf{z}}^{i-1})\mathbf{U}_r)\bar{\mathbf{z}}^i - \\ \quad - \Delta t_i^{-1}\mathbf{V}^T\mathbf{M}\mathbf{U}_r\bar{\mathbf{z}}^{i-1} - \mathbf{V}^T\mathbf{d}^i = 0, \quad i \geq 2 \end{cases} \quad (21)$$

Note that we add an overbar to the variable  $\mathbf{z}$  to distinguish the solution of the hyper-reduced-order model (21) from that of the state-only reduced-order model in equation (17). We will refer to equation (21) with DEIM as POD-DEIM below and POD-GPOD when the hyper-reduction is done with gappy POD.

**Remark 2.** *It can be shown that equation (21) with (20) using either DEIM or gappy POD is consistent with respect to (17) given appropriate assumptions on the time step selection and invertibility of the matrices  $\mathbf{V}^T \mathbf{A}^i \mathbf{U}_r + \mathbf{G} \mathbf{P}^T \mathbf{N}(\mathbf{U}_r \mathbf{z}^{i-2}, \mathbf{U}_r \mathbf{z}^{i-1}) \mathbf{U}_r$ . That is, if the untruncated basis  $\mathbf{W}$  is used on place of  $\mathbf{W}_r$  in matrix  $\mathbf{G}$  in equation (21), then  $\bar{\mathbf{z}}^i = \mathbf{z}^i$ .*

A fine-scale analog of (20) for the collection of nonlinearity snapshots can be used:

$$\mathbf{T}_{fs}^G = (\mathbf{N}_0(\mathbf{v}^0) \mathbf{v}^1, \mathbf{N}(\mathbf{v}^0, \mathbf{v}^1) \mathbf{v}^2, \dots, \mathbf{N}(\mathbf{v}^{M-2}, \mathbf{v}^{M-1}) \mathbf{v}^M) \quad (22)$$

Although it loses the consistency property and introduces irreducible error even if the untruncated basis  $\mathbf{W}_{fs}$  (obtained from an SVD applied to  $\mathbf{T}_{fs}^G$ ) is used in the hyper-reduced model, this strategy is computationally more economical because it does not require simulation of the state-reduced (NPOD) model (17) with fixed  $\mathbf{U}_r$  during the offline stage.

### 3.3 Hyper-reduction for the Petrov-Galerkin projection model

In this section, we follow the same hyper-reduction approach settling on the expansion of the term being reduced through its empirical basis  $\mathbf{W}$  and evaluating only a subset of its rows specified by the matrix  $\mathbf{P}$ . The hyper-reduction applied to the Petrov-Galerkin (PG-NPOD) projection (18), however, differs from the Galerkin hyper-reduced model discussed above in two ways. First, if we aim to drop dependence of complexity of the solution on the fine-scale dimension, we are limited in our choice for the correct term to reduce. Second, the sufficient conditions for consistency of reduction are more strict than for the Galerkin-based model and in practice may be infeasible or at least impracticable. We consider these two issues below.

#### 3.3.1 Proper choice of the reduction term

Assume we are aiming at performing hyper-reduction for the PG-NPOD model in equation (18). Whether we solve this minimization problem via QR-decomposition or transforming to a system of normal equations, the only way to reduce the computational complexity is by dropping the size of the total LHS matrix. Consider, for example, QR-decomposition of the LHS matrix in (18). If the reduction is performed on the vector  $\mathbf{N} \mathbf{U}_r \mathbf{z}^i$  only, the high dimension  $N$  in the complexity of the QR-factorization process still emanates from the matrix  $\mathbf{A}^i$ :

$$(\mathbf{A}^i + \mathbf{N}(\mathbf{U}_r \mathbf{z}^{i-2}, \mathbf{U}_r \mathbf{z}^{i-1})) \mathbf{U}_r \mathbf{z}^i \approx (\mathbf{A}^i + \mathbf{W}_r (\mathbf{P}^T \mathbf{W}_r)^+ \mathbf{P}^T \mathbf{N}(\mathbf{U}_r \mathbf{z}^{i-2}, \mathbf{U}_r \mathbf{z}^{i-1})) \mathbf{U}_r \mathbf{z}^i$$

Therefore, the following reduction is proposed:

$$(\mathbf{A}^i + \mathbf{N}(\mathbf{U}_r \mathbf{z}^{i-2}, \mathbf{U}_r \mathbf{z}^{i-1})) \mathbf{U}_r \mathbf{z}^i \approx \mathbf{W}_r (\mathbf{P}^T \mathbf{W}_r)^+ \mathbf{P}^T (\mathbf{A}^i + \mathbf{N}(\mathbf{U}_r \mathbf{z}^{i-2}, \mathbf{U}_r \mathbf{z}^{i-1})) \mathbf{U}_r \mathbf{z}^i.$$

Then, since  $\mathbf{W}_r$  consists of orthonormal columns, the minimization problem

$$\mathbf{z}^i = \underset{\mathbf{z} \in \mathbb{R}^m}{\operatorname{argmin}} \left\| \mathbf{W}_r (\mathbf{P}^T \mathbf{W}_r)^+ \mathbf{P}^T (\mathbf{A}^i + \mathbf{N}(\mathbf{U}_r \mathbf{z}^{i-2}, \mathbf{U}_r \mathbf{z}^{i-1})) \mathbf{U}_r \mathbf{z} - \Delta t_i^{-1} \mathbf{M} \mathbf{U}_r \mathbf{z}^{i-1} - \mathbf{d}^i \right\|$$

is equivalent to the problem

$$\mathbf{z}^i = \underset{\mathbf{z} \in \mathbb{R}^m}{\operatorname{argmin}} \left\| (\mathbf{P}^T \mathbf{W}_r)^+ \mathbf{P}^T (\mathbf{A}^i + \mathbf{N}(\mathbf{U}_r \mathbf{z}^{i-2}, \mathbf{U}_r \mathbf{z}^{i-1})) \mathbf{U}_r \mathbf{z} - \Delta t_i^{-1} \mathbf{W}_r^T \mathbf{M} \mathbf{U}_r \mathbf{z}^{i-1} - \mathbf{W}_r^T \mathbf{d}^i \right\|,$$

in which the high-dimensional cost is removed, since the matrix  $\mathbf{W}_r^T \mathbf{M} \mathbf{U}_r$  is precomputed before the time-integration and evaluation of  $\mathbf{P}^T(\mathbf{A}^i + \mathbf{N}(\mathbf{U}_r \mathbf{z}^{i-2}, \mathbf{U}_r \mathbf{z}^{i-1}))$  scales with the number of sample rows of matrix  $\mathbf{A}^i + \mathbf{N}(\mathbf{U}_r \mathbf{z}^{i-2}, \mathbf{U}_r \mathbf{z}^{i-1})$ .

Therefore, we are bound to record snapshots that are representative of the action of the *whole* LHS matrix on the reduced state to gain consistency. Note that for the above least-squares system to have unique solution, we require that  $n_w \geq m$ , i.e., the number of columns of  $\mathbf{W}_r$  should be larger than or equal to the number of columns of  $\mathbf{U}_r$ . For Galerkin-projection with hyper-reduction, (21), no such restriction was required.

### 3.3.2 Proper choice of a snapshot set

Determining the consistency for a hyper-reduced version of (18) requires comparing the state-reduced (PG-NPOD) solution

$$\mathbf{z}^i = \operatorname{argmin}_{\mathbf{z} \in \mathbb{R}^m} \|(\mathbf{A}^i + \mathbf{N}(\mathbf{U}_r \mathbf{z}^{i-2}, \mathbf{U}_r \mathbf{z}^{i-1}))\mathbf{U}_r \mathbf{z} - \Delta t_i^{-1} \mathbf{M} \mathbf{U}_r \mathbf{z}^{i-1} - \mathbf{d}^i\|$$

and

$$\bar{\mathbf{z}}_i = \operatorname{argmin}_{\mathbf{z} \in \mathbb{R}^m} \|\mathbf{W}(\mathbf{P}^T \mathbf{W})^+ \mathbf{P}^T(\mathbf{A}^i + \mathbf{N}(\mathbf{U}_r \mathbf{z}^{i-2}, \mathbf{U}_r \mathbf{z}^{i-1}))\mathbf{U}_r \mathbf{z} - \Delta t_i^{-1} \mathbf{M} \mathbf{U}_r \mathbf{z}^{i-1} - \mathbf{d}^i\|.$$

For these solutions to be the same, we ask for the matrix of the first problem to be the same as for the second one:

$$\mathbf{W}(\mathbf{P}^T \mathbf{W})^+ \mathbf{P}^T(\mathbf{A}^i + \mathbf{N}(\mathbf{U}_r \mathbf{z}^{i-2}, \mathbf{U}_r \mathbf{z}^{i-1}))\mathbf{U}_r = (\mathbf{A}^i + \mathbf{N}(\mathbf{U}_r \mathbf{z}^{i-2}, \mathbf{U}_r \mathbf{z}^{i-1}))\mathbf{U}_r.$$

These conditions are fulfilled if we require that  $(\mathbf{A}^i + \mathbf{N}(\mathbf{U}_r \mathbf{z}^{i-2}, \mathbf{U}_r \mathbf{z}^{i-1}))\mathbf{U}_r \in \operatorname{range}(\mathbf{W})$ . Therefore, while collecting snapshots during the run with  $M$  time steps of the PG-NPOD model (18), we include columns of  $(\mathbf{A}^i + \mathbf{N}(\mathbf{U}_r \mathbf{z}^{i-2}, \mathbf{U}_r \mathbf{z}^{i-1}))\mathbf{U}_r$  at every time step into the snapshot matrix:

$$\mathbf{T}^{PG,c} = ((\mathbf{A}^1 + \mathbf{N}_0(\mathbf{v}^0))\mathbf{U}_r, (\mathbf{A}^2 + \mathbf{N}(\mathbf{v}^0, \mathbf{U}_r \mathbf{z}^1))\mathbf{U}_r, \dots, (\mathbf{A}^M + \mathbf{N}(\mathbf{U}_r \mathbf{z}^{M-2}, \mathbf{U}_r \mathbf{z}^{M-1}))\mathbf{U}_r) \quad (23)$$

The resulting Petrov-Galerkin, hyper-reduced scheme can then be written

$$\left\{ \begin{array}{l} \text{initial data } \mathbf{v}^0 \text{ given,} \\ \bar{\mathbf{z}}^1 = \operatorname{argmin}_{\mathbf{z} \in \mathbb{R}^m} \|\mathbf{H} \mathbf{P}^T(\mathbf{A}^1 + \mathbf{N}_0(\mathbf{v}^0))\mathbf{U}_r \mathbf{z} - \Delta t_1^{-1} \mathbf{W}_r^T \mathbf{M} \mathbf{v}^0 - \mathbf{W}_r^T \mathbf{d}^1\|, \\ \bar{\mathbf{z}}^i = \operatorname{argmin}_{\mathbf{z} \in \mathbb{R}^m} \|\mathbf{H} \mathbf{P}^T(\mathbf{A}^i + \mathbf{N}(\mathbf{U}_r \bar{\mathbf{z}}^{i-2}, \mathbf{U}_r \bar{\mathbf{z}}^{i-1}))\mathbf{U}_r \mathbf{z} - \\ \quad - \Delta t_i^{-1} \mathbf{W}_r^T \mathbf{M} \mathbf{U}_r \bar{\mathbf{z}}^{i-1} - \mathbf{W}_r^T \mathbf{d}^i\|, \quad i \geq 2, \end{array} \right. \quad (24)$$

where  $\mathbf{H} = (\mathbf{P}^T \mathbf{W}_r)^+$  denotes a general Moore-Penrose pseudoinverse of the  $l_w \times n_w$  matrix  $\mathbf{P}^T \mathbf{W}_r$  with  $m \leq n_w \leq l_w \leq N$ , and the index selection matrix  $\mathbf{P}$  contains indices from either DEIM or gappy POD.

**Remark 3.** The collection in (23) is the analog of snapshot selection strategy 3 in [12]. With it, the semi-implicit Petrov-Galerkin approximation (24) can be shown to be consistent under the assumption that  $(\mathbf{P}^T \mathbf{W}_r)^+ \mathbf{P}^T(\mathbf{A}^i + \mathbf{N}(\mathbf{U}_r \mathbf{z}^{i-2}, \mathbf{U}_r \mathbf{z}^{i-1}))\mathbf{U}_r$  remains non-singular and identical time step sizes are used for the state-reduced and hyper-reduced simulations.

We will refer to (24) as PG-DEIM or PG-GPOD below, depending on the type of hyper-reduction technique used.

In practice, the snapshot collection method in equation (23) may be too storage intensive. In this work, we resort to a less expensive, though not necessarily consistent strategy that saves the action of the matrix on the reduced state. In other words, we propose saving snapshots of the matrix component of the residual inside the argmin operator already evaluated at the minimizing state found from the state-reduced (PG-NPOD) model. This strategy is summarized in form of a new snapshot matrix  $\mathbf{T}^{PG}$ :

$$\mathbf{T}^{PG} = ((\mathbf{A}^1 + \mathbf{N}_0(\mathbf{v}^0))\mathbf{U}_r\mathbf{z}^1, (\mathbf{A}^2 + \mathbf{N}(\mathbf{v}^0, \mathbf{U}_r\mathbf{z}^1))\mathbf{U}_r\mathbf{z}^2, \dots, (\mathbf{A}^M + \mathbf{N}(\mathbf{U}_r\mathbf{z}^{M-2}, \mathbf{U}_r\mathbf{z}^{M-1}))\mathbf{U}_r\mathbf{z}^M) \quad (25)$$

The fine-scale analog for this strategy, which is expected to be even less consistent but cheaper, is

$$\mathbf{T}_{fs}^{PG} = ((\mathbf{A}^1 + \mathbf{N}_0(\mathbf{v}^0))\mathbf{u}^1, (\mathbf{A}^2 + \mathbf{N}(\mathbf{v}^0, \mathbf{v}^1))\mathbf{v}^2, \dots, (\mathbf{A}^M + \mathbf{N}(\mathbf{v}^{M-2}, \mathbf{v}^{M-1}))\mathbf{u}^M) \quad (26)$$

We conclude this section by noting that in case of more than one variable in a system of PDEs, we can perform reduction for each component of the nonlinearity just as was done for reduction of the state in §3.1.4.

## 4 Numerical experiments

To evaluate the Galerkin and Petrov-Galerkin reduced-order models detailed above, we consider two classical test problems. The first is a one-dimensional Burgers equation example, which we use to explore consistency of the reduction schemes in detail. The second is a well-known circular dam break [19]. In both cases, the semi-discrete and discrete systems have the same basic forms (9) and (11), respectively, with the caveat that the Burgers approximation only involves the 11 block.

### 4.1 1D viscous Burgers equation

We begin with Burgers' equation on the unit interval with constant initial and boundary data

$$\begin{cases} \frac{\partial u}{\partial t} + \frac{1}{2} \frac{\partial u^2}{\partial x} - \nu \frac{\partial^2 u}{\partial x^2} = 0, & x \in (0, 1), t > 0 \\ u(0, t) = 1, & t \geq 0, \\ \nu \frac{\partial u}{\partial x} \Big|_{x=1} = 0, & t \geq 0, \\ u(x, 0) = 0, & x > 0. \end{cases} \quad (27)$$

For the computational mesh, we use  $N = 101$  uniformly spaced nodes. We set the viscosity to  $\nu = 0.01$  and time step to  $\Delta t = 0.01$ .

#### 4.1.1 Galerkin-based state reduction

We first perform a fine-scale run until  $T = 2$  to collect the state snapshots. If we perform a non-thin SVD on the snapshot set, we produce a basis  $\mathbf{U}$  that reaches the fine-scale dimension  $N$ . The singular values in log-scale are shown in Fig. 1. We also measure the relative error in the state-reduced solution

$$\varepsilon_{POD} = \frac{\max_i \|\mathbf{v}^i - \mathbf{U}_r\mathbf{z}^i\|_2}{\max_i \|\mathbf{v}^i\|_2} \quad (28)$$

for each simulation. Fig. 2 plots  $\varepsilon_{POD}$  against the number of modes  $m$  for the state variable  $u$ . The lowest error value achieved over the modal spectrum  $1 \leq m \leq 50$  is approximately  $3.4 \cdot 10^{-5}$ . The graphs of the fine-scale and Galerkin-based reduced-order (NPOD) solution are shown for two instances of time in Figs. 3 and 4.

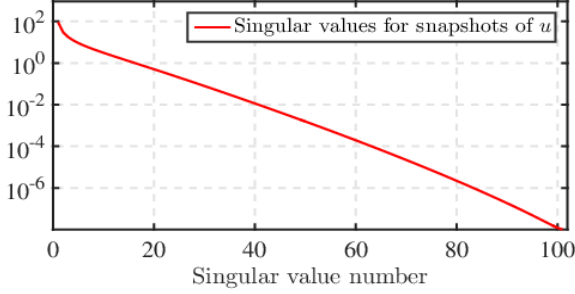


Figure 1: Singular values for state,  $u$ .

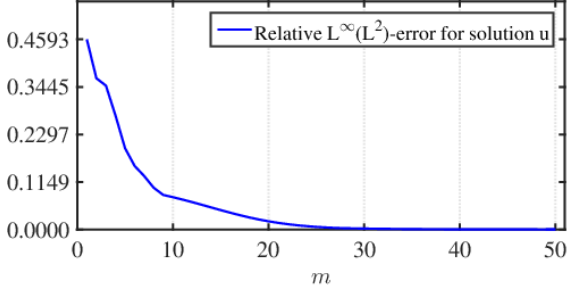


Figure 2:  $\varepsilon_{POD}$

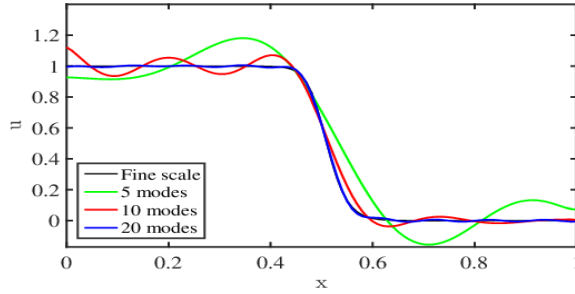


Figure 3: Solution curves at  $t = 1$

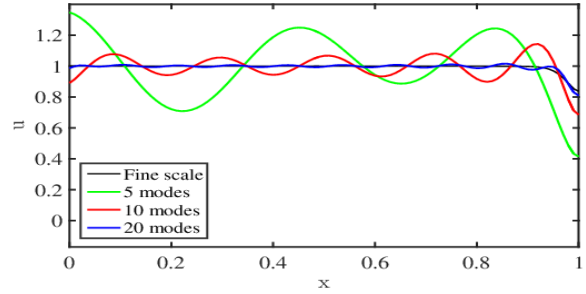


Figure 4: Solution curves at  $t = 2$

#### 4.1.2 Galerkin-based hyper-reduction

Next, the reduced-order model with hyper-reduction is investigated. During the fine-scale run of the previous subsection, the nonlinearity snapshots

$$\mathbf{T}_{fs}^G = (\mathbf{N}(\mathbf{v}^0)\mathbf{v}^1, \mathbf{N}(\mathbf{v}^1)\mathbf{v}^2, \dots, \mathbf{N}(\mathbf{v}^{199})\mathbf{v}^{200})$$

were collected. During the state-reduced NPOD run with  $m = 10$  modes ( $\mathbf{U}_r \in \mathbb{R}^{101 \times 10}$ ) we additionally collected snapshots as shown:

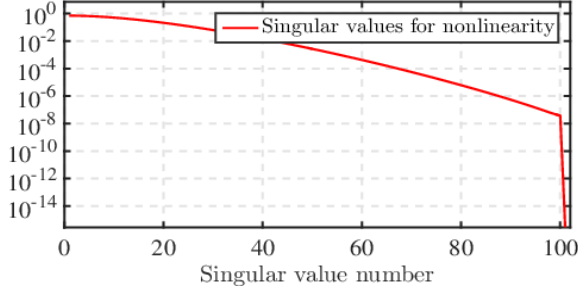
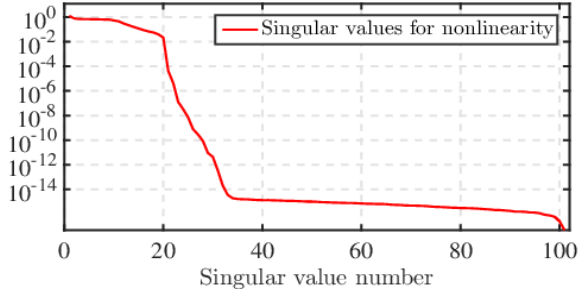
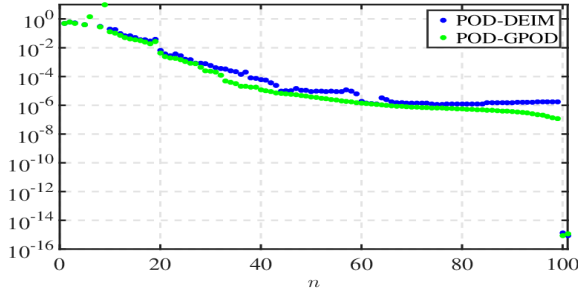
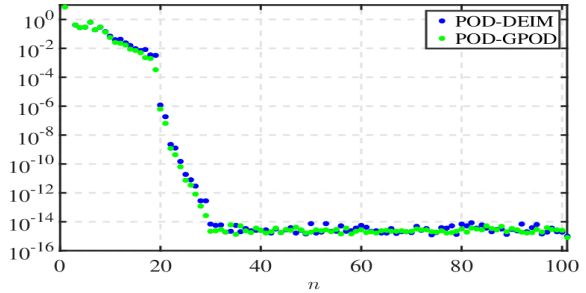
$$\mathbf{T}^G = (\mathbf{N}(\mathbf{v}^0)\mathbf{U}_r\mathbf{z}^1, \mathbf{N}(\mathbf{U}_r\mathbf{z}^1)\mathbf{U}_r\mathbf{z}^2, \dots, \mathbf{N}(\mathbf{U}_r\mathbf{z}^{199})\mathbf{U}_r\mathbf{z}^{200})$$

Empirical bases were found via SVD and are denoted as  $\mathbf{W}_{fs}$  and  $\mathbf{W}$ , respectively. Their singular values in log-scale are shown in Figs. 5 and 6.

DEIM and gappy POD sample index selection algorithms from [20] were applied to both, and the hyper-reduced models were constructed and tested. During the hyper-reduced simulations, the relative error between the hyper-reduced and NPOD solutions

$$\varepsilon_{hyp} = \frac{\max_i \|\mathbf{U}_r\mathbf{z}^i - \mathbf{U}_r\bar{\mathbf{z}}^i\|_2}{\max_i \|\mathbf{U}_r\mathbf{z}^i\|_2} = \frac{\max_i \|\mathbf{z}^i - \bar{\mathbf{z}}^i\|_2}{\max_i \|\mathbf{z}^i\|_2} \quad (29)$$

was recorded for varying  $\mathbf{W}_r$ . The results are shown in Figs. 7 and 8.

Figure 5:  $\mathbf{T}_{fs}^G$  singular valuesFigure 6:  $\mathbf{T}^G$  singular valuesFigure 7:  $\varepsilon_{hyp}$  for  $\mathbf{T}_{fs}^G$ Figure 8:  $\varepsilon_{hyp}$  for  $\mathbf{T}^G$ 

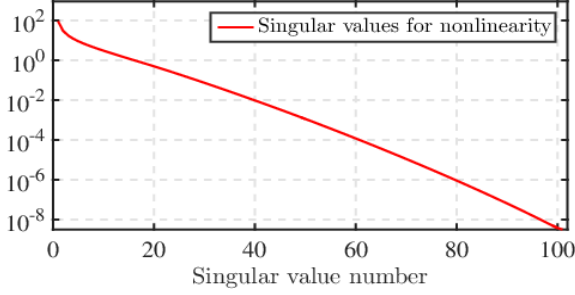
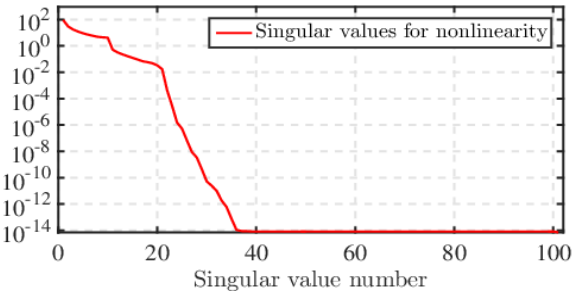
We observe the following. First, the consistency of the model with the fine-scale-based snapshot set  $\mathbf{T}_{fs}^G$  is only achieved by reaching the fine-scale dimension for the nonlinearity, which is a trivial case of consistency, since this corresponds to an isomorphic change of the degrees of freedom. In other words, since the basis  $\mathbf{W}_{fs}$  is less representative of the nonlinearity recorded in  $\mathbf{T}^G$  than  $\mathbf{W}$ , the error stagnates before the rank of the  $\mathbf{T}_{fs}^G$  is reached (the rank is  $m = N - 1$  due to the constant Dirichlet boundary condition, as is also confirmed by Fig. 5). Second, the decay of the singular values toward machine precision at around  $n_w \approx 32$  for  $\mathbf{T}^G$ , shown in Fig. 6 implies that the basis captures the nonlinearity throughout the simulation at this number of modes. We then see the expected drop in error to machine precision with  $n_w \approx 32$  when using  $\mathbf{T}^G$  as the snapshot set. Third, we see overall better accuracy of the gappy POD hyper-reduction strategy as opposed to DEIM, which is consistent with the results in [20]. Qualitatively similar graphs were obtained when  $\mathbf{U}_r$  had  $m = 5$  and 20 columns for the state reduction.

#### 4.1.3 Petrov-Galerkin-based state reduction

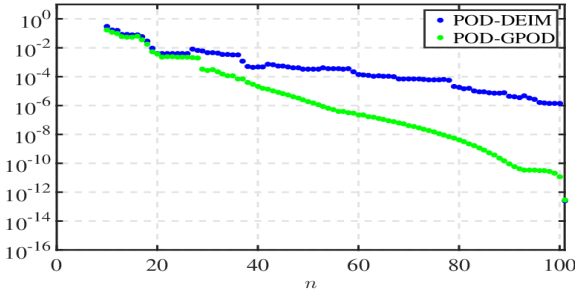
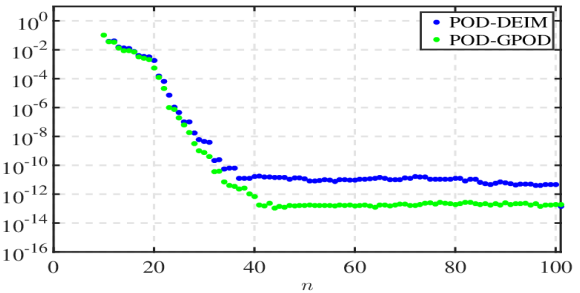
We next consider the Petrov-Galerkin model without hyper-reduction (PG-NPOD). We use the same bases  $\mathbf{U}$  for the state  $\mathbf{v}$  as for the NPOD model, i.e., those obtained during the fine-scale run of (27) with final time  $T = 2$ . The solution curves obtained from the PG-NPOD model (not shown) were comparable to those presented in Figs. 3-4, for 5, 10, and 20 modes. We again calculated the relative  $L^\infty(0, T; L^2)$ -error (28) for the changing number of state modes,  $m$ , between 1 and 50. The lowest error value occurred when  $m = 50$  and was equal to  $3.4 \cdot 10^{-5}$ . For the relatively smooth solution behavior in Fig. 3-4, the differences in accuracy between the NPOD and PG-NPOD approximations were negligible.

#### 4.1.4 Petrov-Galerkin-based hyper-reduction

We finally try hyper-reduction for the Petrov-Galerkin reduced model given by equation (24). This time, we collected the nonlinearity snapshots  $\mathbf{T}_{fs}^{PG}$  via (26) from the fine-scale runs, and  $\mathbf{T}^{PG}$  from (25) using  $m = 10$  during the state-reduced (PG-NPOD) runs. From these, we again used SVD to obtain the bases  $\mathbf{W}_{fs}$  and  $\mathbf{W}$ , respectively. The singular values are shown in Figs. 9 and 10, respectively. The errors (29) coming from the runs of the hyper-reduced models,

Figure 9:  $\mathbf{T}_{fs}^{PG}$  singular valuesFigure 10:  $\mathbf{T}^{PG}$  singular values

PG-DEIM and PG-GPOD, are presented in Figs. 11 and 12. Note that in the figures, the modal range starts with  $n_w = m = 10$ , due to the restriction that the hyper-reduced model have a unique least-squares solution.

Figure 11:  $\varepsilon_{hyp}$  for  $\mathbf{T}_{fs}^{PG}$ Figure 12:  $\varepsilon_{hyp}$  for  $\mathbf{T}^{PG}$ 

Unlike the Galerkin-based models, here neither of the snapshot sets guarantees consistency, unless the entire basis is exhausted. Indeed, the drop to machine precision for the fine-scale snapshot set  $\mathbf{T}_{fs}^{PG}$  occurs only when the fine-scale dimension is reached. The basis  $\mathbf{W}_{fs}$  with gappy POD predicts the solution from the Petrov-Galerkin state-reduced model (PG-NPOD) much better than when the DEIM technique is used. The results with  $\mathbf{T}^{PG}$  are much better with both hyper-reduction techniques, although the DEIM error curve demonstrates a small irreducible error even after reaching the effective rank of  $\mathbf{T}^{PG}$ , unlike gappy POD, which manages to reach machine precision accuracy even though the snapshot set  $\mathbf{T}^{PG}$  is not (provably) consistent.

## 4.2 2D shallow water

In this section, the FEM scheme from equation (9) discretized in time via (11) is used for the simulation of an SWE problem, for which the geometry, topography, and the initial conditions were taken from [19]. The domain is a square  $[0, 50] \times [0, 50]$ , meshed uniformly by 20,000

equal triangles having sides  $1/2$ ,  $1/2$  and  $\sqrt{2}/2$ . This mesh generates  $N_n = 10201$  nodes in total, and that results in three times as many, i.e.,  $N = 30603$  degrees of freedom for the entire FEM-discretized system. The topography function  $b \equiv -1$  throughout the domain with gravity  $g = 9.81$ , and we additionally set  $\nu = 10^{-4}$  for viscosity and  $n_{mn} = 1.5 \cdot 10^{-4}$  for the Manning coefficient. For the initial conditions, the elevation was given in a form of a cylindrical dam in the center of the square. In terms of depth,

$$u_1^0 = \begin{cases} 10, & \text{for } \sqrt{(x-25)^2 + (y-25)^2} \leq 11, \\ 1, & \text{otherwise} \end{cases}$$

and  $u_2^0 = u_3^0 = 0$ . Finally, wall boundary boundary conditions were assumed on all four sides

The discontinuity implied by the initial condition is expected to be handled during the time integration by the shock-capturing term that is incorporated in the scheme (9). As time evolution develops, the dam breaks into a wave traveling radially from the center of the square, and then reflects from the boundaries. The fine-scale simulation, as well as the subsequent reduced-order simulations, were performed with  $\Delta t = 0.005$  until  $T = 5$ , which corresponds to 1000 steps. The results of the fine-scale simulation for different time instances are shown in Figs. 13–16. Since the depth in the fine solution remains bounded well away from 0 (the vacuum or dry state)

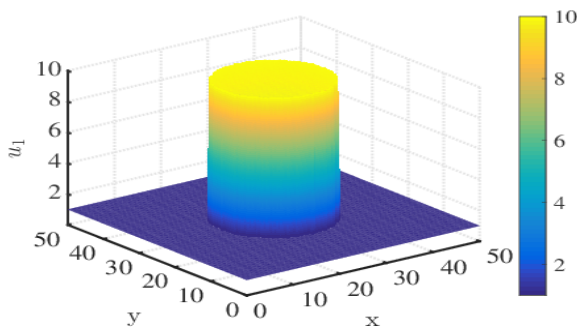


Figure 13: Initial depth

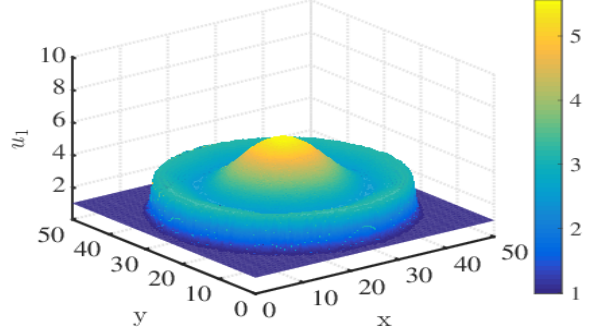


Figure 14: Depth at  $t = 1.25$

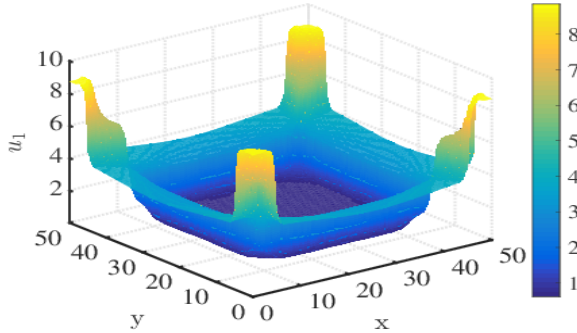


Figure 15: Depth at  $t = 3.5$

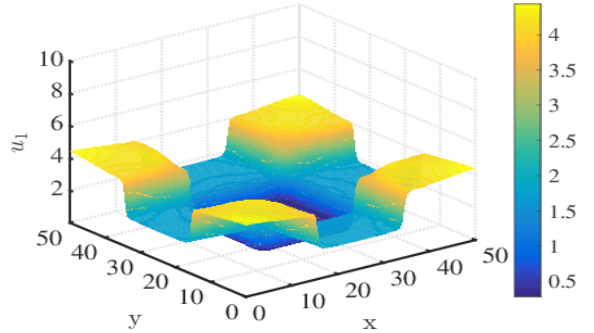


Figure 16: Depth at  $t = 5$ (final time)

in the fine scale simulations, we require that the various model reduction techniques considered maintain  $h \geq 0$ . Otherwise, we mark the simulation as failed, rather than engage a wetting and drying routine.

During the fine-scale simulations, state snapshots,  $\mathbf{S}$ , were collected separately for each solution component. The nonlinear snapshots  $\mathbf{T}_{fs}^G$  and  $\mathbf{T}_{fs}^{PG}$  were also collected separately for each equation in the SWE system. We will use a superscript  $i = 1, 2, 3$  to distinguish the snapshot matrices when necessary below.



While calculations were performed with both the Galerkin and Petrov-Galerkin reduced models, we present only the Petrov-Galerkin results below for brevity. As before, the SVD bases calculated from  $\mathbf{T}_{fs}^{PG}$  will be denoted  $\mathbf{W}_{fs}^i$  with corresponding index  $1 \leq i \leq 3$ , while those from  $\mathbf{T}^{PG}$  will be denoted  $\mathbf{W}^i$ .

#### 4.2.1 State-reduced Petrov-Galerkin model

The solution snapshots for each of the three variables were decomposed via SVD to obtain bases  $\mathbf{U}_1, \mathbf{U}_2, \mathbf{U}_3$ , all of size  $10201 \times 1000$ , for these variables respectively. The global basis is then made of  $\mathbf{U}_i$  placed along the diagonal block-wise, as in (19). We can then write the PG-NPOD update at each time step as

$$\begin{pmatrix} \mathbf{z}_1 \\ \mathbf{z}_2 \\ \mathbf{z}_3 \end{pmatrix}^k = \underset{\mathbf{z} \in \mathbb{R}^{3m}}{\operatorname{argmin}} \left\| \left( \mathbf{A}^k + \mathbf{N}^{k-1,k-2} \right) \mathbf{U}_r \mathbf{z} - \frac{1}{\Delta t_k} \mathbf{M} \mathbf{U}_r \begin{pmatrix} \mathbf{z}_1 \\ \mathbf{z}_2 \\ \mathbf{z}_3 \end{pmatrix}^{k-1} \right\|. \quad (30)$$

The depth solution obtained from the PG-NPOD scheme with  $m = 50$  is shown in Figs. 17 and 18, together with absolute values of the components of  $\mathbf{v}_1 - \mathbf{U}_{1,r} \mathbf{z}_1$  for depth at the same time instances. The similarity of Figs. 17-18 to the fine-scale solution Figs. 14-16 is apparent. The relative error for the depth  $h = \mathbf{u}_1$ ,  $L^\infty$  in time and  $L^2$  in space,  $\varepsilon_{POD}$ , was 0.0504.

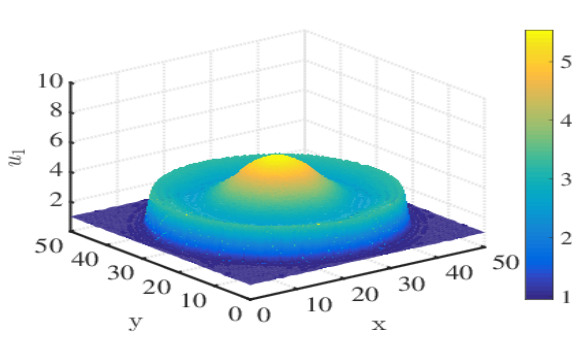


Figure 17: PG-NPOD solution at  $t = 1.25$

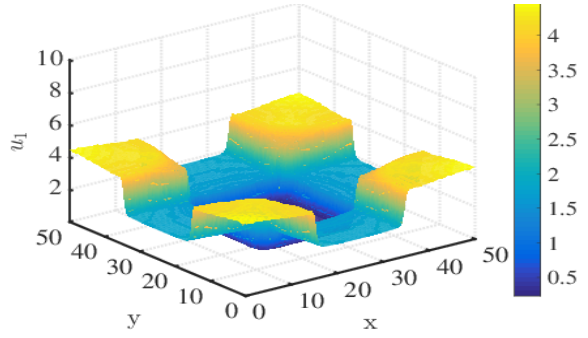


Figure 18: PG-NPOD solution at final time  $t = 5$

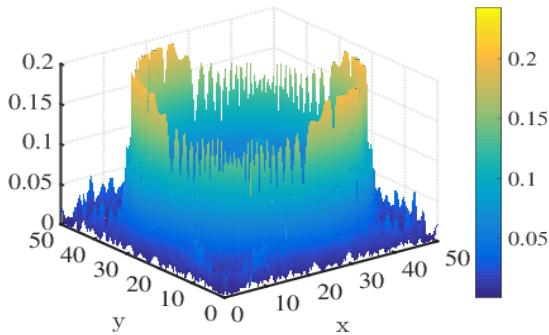


Figure 19: PG-NPOD absolute error at  $t = 1.25$

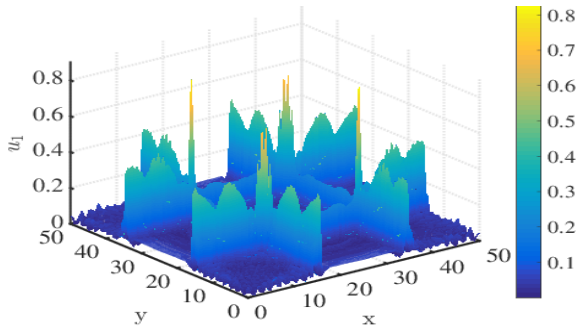


Figure 20: PG-NPOD absolute error at  $t = 5$

#### 4.3 Hyper-reduction

Four scenarios in total were used for the hyper-reduction assessment of the Petrov-Galerkin (GNAT-based) scheme. We considered: DEIM and gappy POD for  $\mathbf{T}_{fs}^{PG}$  computed from the

fine-scale simulations as well as  $\mathbf{T}^{PG}$  computed from PG-NPOD simulations with  $m = 50$  modes for each component of the state variable,  $\mathbf{u}$ . In other words, we had a reduced basis for each state component,  $\mathbf{U}_i \in \mathbb{R}^{10201 \times 50}$ ,  $i = 1, 2, 3$ . We used the same number of nonlinear modes,  $n_w$ , for each snapshot basis  $\mathbf{W}^i$  and  $\mathbf{W}_{fs}^i$  for  $i = 1, 2, 3$ , and  $50 \leq n_w \leq 1000$ . We again measured the error (29) as before but for simplicity report only the error for the depth variable,  $u_1$ .

#### 4.3.1 Petrov-Galerkin projection approximation

The DEIM method did not perform well for the bases  $\mathbf{W}_{fs}$ . No simulation completed the full simulation to  $T = 5$  without violating the depth-positivity constraint for  $n_w$  in the range  $50 \leq n_w \leq 1000$ . The results with using  $\mathbf{T}^{PG}$  were slightly better. Within the range  $50 \leq n_w \leq 1000$  sampled in increments of 10, six runs successfully completed the simulation. The errors for these runs are shown in Table 4.3.1. Note, the error values are multiplied by 100.

# of hyper-modes $n_w$	210	230	520	550	650	740
error $\varepsilon_{hyp} \cdot 10^2$	6.36	6.53	4.587	5.12	2.5	2.86

Table 1:  $\varepsilon_{hyp}$  for PG-DEIM using snapshots  $\mathbf{T}^{PG}$

As with DEIM, gappy POD hyper-reduction for the fine-scale bases  $\mathbf{W}_{fs}$ , did not produce a simulation that completed to  $T = 5$  without violating the positivity constraint. On the other hand, gappy POD hyper-reduction using the bases  $\mathbf{W}$  obtained from the PG-NPOD simulations was significantly better, showing both higher accuracy and more robustness. The relative error,  $\varepsilon_{hyp}$ , for  $10 \leq n_w \leq 1000$  (sampled in multiples of 10) is shown in Fig. 21.

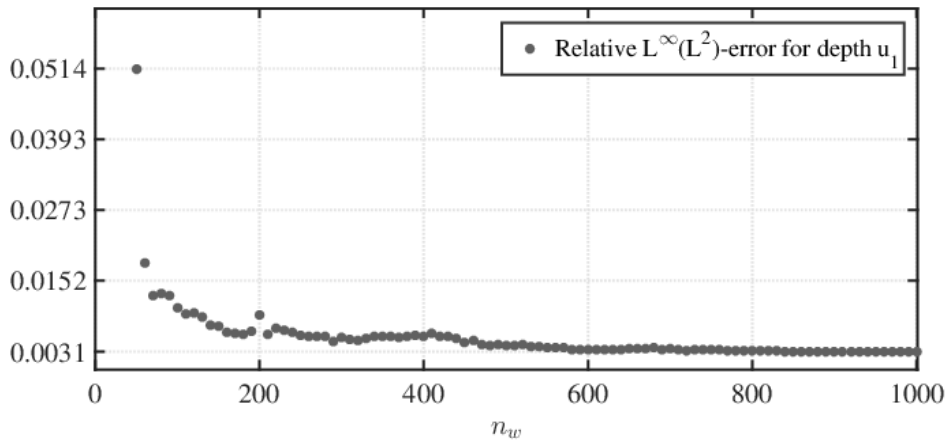


Figure 21:  $\varepsilon_{hyp}$  for the PG-GPOD model with varying number of empirical modes,  $n_w$

## 5 CONCLUSION

In this work, we presented a fine-scale scheme for the SWE based on a stabilized FEM approximation and semi-implicit time integration. We then formulated reduced-order models

for this approximation based on both Galerkin and Petrov-Galerkin projection. We introduced hyper-reduction to the models via both DEIM and gappy POD techniques and considered alternative snapshot selection strategies and their consistency.

We performed two sets of numerical experiments to explore the schemes' performance. Numerical experiments for viscous Burgers equation clearly supported theoretical predictions concerning consistency of both the Galerkin and Petrov-Galerkin frameworks. The shallow water example was significantly more challenging but confirmed the trends observed in the Burgers equation results. Specifically,

- Irreducible errors were observed in all scenarios when a basis generated from fine-scale simulations directly was used.
- For Galerkin projection, the consistency predictions were confirmed by simulations with untruncated bases that were constructed from NPOD computations.
- Gappy POD hyper-reduction was more robust than DEIM in both the Galerkin and Petrov-Galerkin frameworks.
- The POD-GPOD and PG-GPOD approximations using snapshots  $\mathbf{T}^G$  and  $\mathbf{T}^{PG}$ , respectively, are the best candidates for robust online solvers in sharp-front SWE problems like the dam-break example considered here.

## References

- [1] V. Aizinger and C. N. Dawson. A discontinuous Galerkin method for two-dimensional flow and transport in shallow water. *Advances in Water Resources*, 25(1):67–84, 2002.
- [2] D. Amsallem, M. Zahr, Y. Choi, and C. Farhat. Design optimization using hyper-reduced-order models. *Structural and Multidisciplinary Optimization*, 51(4):919–940, 2015. ISSN 1615-147X. doi: 10.1007/s00158-014-1183-y. URL <http://dx.doi.org/10.1007/s00158-014-1183-y>.
- [3] A.C. Antoulas. *Approximation of large-scale dynamical systems*, volume 6. SIAM, 2005.
- [4] A.C. Antoulas and D.C. Sorensen. Approximation of large-scale dynamical systems: An overview. *International Journal of Applied Mathematics and Computer Science*, 11(5): 1093–1121, 2001.
- [5] M. Barrault, Y. Maday, N.C. Nguyen, and A.T. Patera. An empirical interpolation method: application to efficient reduced-basis discretization of partial differential equations. *Comptes Rendus Mathematique*, 339(9):667–672, 2004.
- [6] P. Benner, S. Gugercin, and K. Willcox. A survey of projection-based model reduction methods for parametric dynamical systems. *SIAM Review*, 57(4):483–531, 2015.
- [7] S.W. Bova and G.F. Carey. A symmetric formulation and SUPG scheme for the shallow-water equations. *Advances in Water Resources*, 19(3):123–131, 1996.
- [8] E. Burman and A. Ern. Nonlinear diffusion and discrete maximum principle for stabilized Galerkin approximations of the convection-diffusion-reaction equation. *Computer Methods in Applied Mechanics and Engineering*, 191:3833–3855, 2002.

- [9] T. Butler, L. Graham, D. Estep, C.N. Dawson, and J.J. Westerink. Definition and solution of a stochastic inverse problem for the Mannings  $n$  parameter field in hydrodynamic models. *Advances in Water Resources*, 78:60–79, 2015.
- [10] M.A. Cardoso, L.J. Durlofsky, and P. Sarma. Development and application of reduced-order modeling procedures for subsurface flow simulation. *International Journal for Numerical Methods in Engineering*, 77(9):1322–1350, 2009.
- [11] K. Carlberg, Charbel B.-M., and C. Farhat. Efficient non-linear model reduction via a least-squares Petrov–Galerkin projection and compressive tensor approximations. *International Journal for Numerical Methods in Engineering*, 86(2):155–181, 2011.
- [12] K. Carlberg, C. Farhat, and D. Amsallem. The GNAT method for nonlinear model reduction: effective implementation to computational fluid dynamics and turbulent flows. *Journal of Computational Physics*, 242:623–647, 2013.
- [13] S. Chaturantabut and D.C. Sorensen. Nonlinear model reduction via discrete empirical interpolation. *SIAM Journal on Scientific Computing*, 32(5):2737–2764, 2010.
- [14] R. Everson and L. Sirovich. Karhunen-Loève procedure for gappy data. *Journal of the Optical Society of America A*, 12(8):1657–1664, 1995.
- [15] T.J.R. Hughes and M. Mallet. A new finite element formulation for computational fluid dynamics: III. The generalized streamline operator for multidimensional advective-diffusive systems. *Computer Methods in Applied Mechanics and Engineering*, 58(3):305–328, 1986.
- [16] T.J.R. Hughes, G.R. Feijóo, L. Mazzei, and J.-B. Quincy. The variational multiscale method – a paradigm for computational mechanics. *Computer Methods in Applied Mechanics and Engineering*, 166(1):3–24, 1998.
- [17] W. Hundsdorfer and J. G. Verwer. *Numerical solution of time-dependent advection-diffusion-reaction equations*. Springer-Verlag Publishers, Berlin, Germany, 2003.
- [18] R. J. LeVeque. *Finite Volume Methods for Hyperbolic Problems*. Cambridge University Press, New York, NY, 2002.
- [19] R. Liska and B. Wendroff. 2d shallow water equations by composite schemes. *International Journal for Numerical Methods in Fluids*, 30(4):461–479, 1999.
- [20] A. Lozovskiy, M.W. Farthing, C.E. Kees, and E. Gildin. POD-based model reduction for stabilized finite element approximations of shallow water flows. *Journal of Computational and Applied Mathematics*, page In press, 2016.
- [21] P. Ortiz. Non-oscillatory continuous FEM for transport and shallow water flows. *Computer Methods in Applied Mechanics and Engineering*, 223–224:55–69, 2012.
- [22] C.B. Vreugdenhil. *Numerical methods for shallow-water flow*. Kluwer Academic Publishers, 1992.
- [23] K. Willcox. Unsteady flow sensing and estimation via the gappy Proper Orthogonal Decomposition. *Computers and Fluids*, 35(2):208–226, 2006.